
Article:
Zhu, Z, Chen, Z, Lin, G et al. (5 more authors) (2019) Buckled Amorphous Hollow Carbon Spheres: Facile Fabrication, Buckling Process and Applications as Electrode Materials for Supercapacitor. ACS Applied Materials & Interfaces, 11 (33). pp. 30116-30124. ISSN 1944-8244

https://doi.org/10.1021/acsami.9b07412

Buckled Amorphous Hollow Carbon Spheres: Facile Fabrication, Buckling Process and Applications as Electrode Materials for Supercapacitor

Zhifeng Zhu[1]‡, Ze Chen[1]‡, Gaojian Lin[3], Yuanhang Ge[1], Yingfeng Tu[1], Hui Chen[1], Sunjie Ye[2], and Xiaoming Yang[1, 4]**

[1] State and Local Joint Engineering Laboratory for Novel Functional Polymeric Materials, Suzhou Key Laboratory of Macromolecular Design and Precision Synthesis, Jiangsu Key Laboratory of Advanced Functional Polymer Design and Application, Department of Polymer Science and Engineering, College of Chemistry, chemical Engineering and Materials Science, Soochow University, Suzhou 215123, P. R. China.

[2] School of Physics and Astronomy, University of Leeds, LS2 9JT, Leeds, UK.

[3] Department of Mechanics Engineering, School of Mechatronical Engineering, Beijing Institute of Technology, Beijing100081, China.

[4] Key Laboratory of Advanced Textile Materials and Manufacturing Technology (Zhejiang Sci-Tech University), Ministry of Education. Hangzhou 310023, China.

‡ These two authors contributed equally to this work.

KEYWORDS: buckled hollow carbon spheres, buckling process, nanoindentation, finite element analyses, supercapacitor

ABSTRACT

Buckled hollow carbon nanospheres (BHCS) integrate several attractive properties desired for a variety of potential applications. However, the development of a feasible and simple method for preparing BHCS nanoparticles remains a great challenge. Herein, we present a facile strategy for fabricating monodisperse BHCSs via the compression of intact hollow carbon nanospheres (HCSs) with improved mechanical strength. The essence of our strategy lies in the successful preparation of robust HCSs that can sustain large mechanical deformation during compression, based on the introduction of polyvinylpyrrolidone in the synthesis of HCS template. Both experiments and finite element analyses are conducted to probe deformation mechanism of buckling, suggesting the residual stress introduced by pyrolysis of precursors plays a predominant role in the buckling process. Furthermore, the use of BHCSs as high-performance supercapacitors is demonstrated. Our work provides important insights in the engineering of robust amorphous carbon nanomaterials by template method and mechanical modulation, and provides an innovative synthetic strategy for fabricating asymmetric hollow spheres with potential for a diversity of applications.

INTRODUCTION

Micro/nano hollow spheres have received numerous concerns due to their excellent properties such as large specific surface area, low density, permeability shell and accommodation of guest molecules.[1] As a result, micro/nano hollow spheres have played important roles in the applications of coating, papermaking, and cosmetic. However, a majority of hollow spheres possess intact hollow spherical structure because of their minimum interfacial free energy. Recently, many efforts have been devoted to designing and constructing asymmetric hollow spheres, because they reduce the excessive hollow interior space while retaining the prevalent advantages of hollow structures.[2-4] Generally, there are mainly three fabrication approaches: 1. template-assisted synthesis, whereby hollow particles are prepared by coating a sacrificial core particle with a shell, followed by the decomposition or dissolution of the core.[5-8] For instance, Lou et al. fabricated bowl-like SnO_2@carbon hollow particles using buckled polystyrene particles as templates.[9] 2. Swelling and phase separation techniques.[10] For example, Masayoshi Okubo et al. produced PMMA (polymethyl methacrylate)/PS (polystyrene) particles with dents on their surface by phase separation between PS and PMMA.[11] 3. Seeded emulsion polymerization, which is a traditional and typical way for the preparation of spherical and nonspherical latex particles, enabling the control of anisotropic particles not only in shapes but also in their chemical and physical properties.[12] Although a series of deformed microcapsules were successfully prepared with the above methods, the size distributions of particles were rather broad and the size of particle was usually in micro and sub-micro scale. Notably, most capsules have shells made of mechanically-flexible polymers, but their uses have been largely limited by the low thermal stability, low conductivity, and chemical incompatibility.

Amorphous hollow carbon nanospheres (HCSs) have attracted much attention in recent years owing to their high thermal stability, high conductivity, high surface area and low density. Furthermore, buckling structures have been demonstrated to endow high stretchability, improved mechanical durability as well as stable electronic performance, and thus have shown potential in a broad range of applications, e.g. energy harvesters, nanogenerators, capacitive or resistive sensors. Therefore, several mechanisms and methods for the formation of buckles have been systematically explored, including substrate molding, prestretch-and-release strategy, deformation induced by solvent or heat and mechanical compression.[13-15] Asymmetric HCSs, especially buckled hollow carbon spheres (BHCSs) have been subject to extensive research interest. In addition to the advantages of HCSs, BHCSs possess increased volumetric packing density and shortened diffusion pathway facilitating mass transport, thus have shown a wide range of applications, such as catalysis, adsorption, sensing, and energy storage.[17] Procedures for the fabrication of HCSs have been reported and tend to involve various templating approaches, but intact and broken HCSs were usually obtained due to their brittle structure. A few examples were reported related to the fabrication of BHCSs which show intelligent drug delivery/releasing property or superior electrochemical performance.[16-18] However, the fabrication method is complicated and case-specific, and the mechanism for the deformed process is not clear. The fabrication of uniformly sized BHCSs via a simple method, and the elucidation of the underlying mechanism for the buckling process remain challenges. Mechanical compression, although a direct and easy-to-operate method for generating buckling structures, has not been employed to prepare BHCSs, mainly due to the breakages and ruptures of the HCS shell caused by the poor structural robustness. Improving the structural robustness of HCSs is essential for enabling the simple fabrication of BHCSs via the compression method.

On the other hand, the mechanical performance of HCSs and corresponding BHCSs is critical for determining the structural integrity of the devices and systems based on HCSs. Understanding the mechanical behavior of HCSs would provide important implications of the fundamental mechanisms on how to improve the structural durability of the devices and systems for engineering applications.[19] To date, there has been little reported work in this field.[20]

Herein, we report the preparation of BHCSs based on the compression of HCSs with structural robustness. In our method, PVP (polyvinylpyrrolidone) and PPy (polypyrrole) were coated on the surface of PS sphere at the same time to build core-shell particles. In the process of pyrolysis, PS was totally removed, the shell consisting of PPy and PVP was carbonized to obtain HCSs with structural robustness. BHCSs were prepared by the compression of robust HCSs. Experiments and detailed finite element analyses (FEA) are performed to understand the buckling process of the HCSs. Moreover, the use of the BHCSs as high-performance supercapacitors electrodes was demonstrated.

RESULTS AND DISCUSSION

Monodisperse PS NPs were used as templates for the synthesis of HCSs and corresponding BHCSs owing to their commercial availability and mature processing technique. In particular, PS NPs of desired size can be readily prepared with a narrow size distribution, enabling a good size control for the resultant HCSs and BHCSs.

Figure 1. **Schematic model of preparing PS@PPy/PVP core-shell NPs, HCSs and corresponding BHCSs.**

Moreover, no etching process is required for template removal, due to the thermal decomposition of PS at 400 ^{0}C.[21-23] However, the HCSs without PVP with low pyrrole (Py) monomer loading (0.1, 0.2, and 0.4 g) exhibit ruptured shells, which results from the intolerance of thin shell to the pyrolysis, caused by its poor mechanical strength (**Figure S1**). Hence, improving the mechanical performance of the shell is important for obtaining intact HCSs and corresponding BHCSs. Interestingly, intact HCSs were obtained by introducing PVP in the process of the interfacial polymerization of Py monomer on the surface of PS NPs. The synthetic route of core-shell NPs and carbonized samples are described in **Figure 1**. PS NPs with diameter of 150.4 ± 8.8 nm showing smooth surface (**Figure S2a and b**) were prepared by emulsion polymerization. PS NPs were prepared by traditional emulsion polymerization. The resulting particles were spherical, monodisperse with a particle size of 150.4 ± 8.8 nm (**Figure S2a and b**), and showing smooth surface. PVP has been conventionally used as an anchoring agent for Py monomer.[24-26] Due to their amphiphilic character (highly polar lactam group and nonpolar alky backbone affording hydrophilicity and hydrophobic property, respectively), PVP chains can be arranged with their nonpolar alkyl backbones anchoring on the surface of hydrophobic PS surface and the polar lactam

group toward the water (**Figure 1**).[27] When Py monomers are added in water, most of them are dispersed as monomer droplets because of their low water solubility, and a small portion of Py monomer is soluble in water. As $FeCl_3$ oxidant is added, Py cation radicals or PPy oligomers can be produced only at the aqueous phase because $FeCl_3$ is water soluble. It is proposed that the electron-rich oxygen atoms on the lactam groups of PVP, with the fractional negative charge of 0.37 could be regarded as the active sites to anchor Py cation radicals for growing PPy oligomers,[28] that is, PVP chains tend to capture *in-situ* formed Py cation radicals. As a result, PPy nucleate at the interface of water and PVP chains. Monomer droplets of Py serve as monomer storage to provide monomer continuously. Finally, PPy shell was formed on the surface of PS NPs to form core-shell NPs (**Figure S3**). HCSs were obtained by heating the core-shell NPs to 900 ^{0}C under nitrogen atmosphere, where PS cores were removed absolutely and PPy shell were carbonized by pyrolysis at the same time (**Figure 1**). It was reported that PVP was completely removed in the process of pyrolysis.[29] However, in this study, a small amount of PVP (3.4%) is found to be retained after pyrolysis (**Figure S4**), which is important for improving the mechanical properties of HCSs (which will be discussed in the following session). Afterwards, BHCSs were prepared from HCSs via a mechanical compression.

TEM and SEM images of the HCSs and corresponding BHCSs with and without PVP are shown in Figure 2 and Figures S5. Strikingly, in the presence of PVP, HCSs having an intact shell (**Figure 2a and c**) with a thickness of 8.8 ± 1.1 nm were obtained. However, under the same synthesis condition, the HCSs prepared without PVP showed shells with a hole (**Figure S5**).[30,31] Interestingly, HCSs with PVP show buckled morphology after being compressed at 11 MPa with a mechanical compression, while HCSs without PVP show broken morphologies under the same conditions (**Figure S5)**. Intriguingly, when the compression pressure was decreased to 8 MPa,

HCSs with PVP did not show obvious change (**Figure S6a**). When the compression pressure was increased from 11 to 15 or 20 MPa, the buckling of same level was observed (**Figure S6b and c**), which means 11 MPa is the critical point of pressure for inducing buckling phenomenon. It is worth noting that, BHCSs in the same batch exhibit different degrees of buckling, which arises from the varied pressure received by each HCS caused by their multilayer and random packing mode.

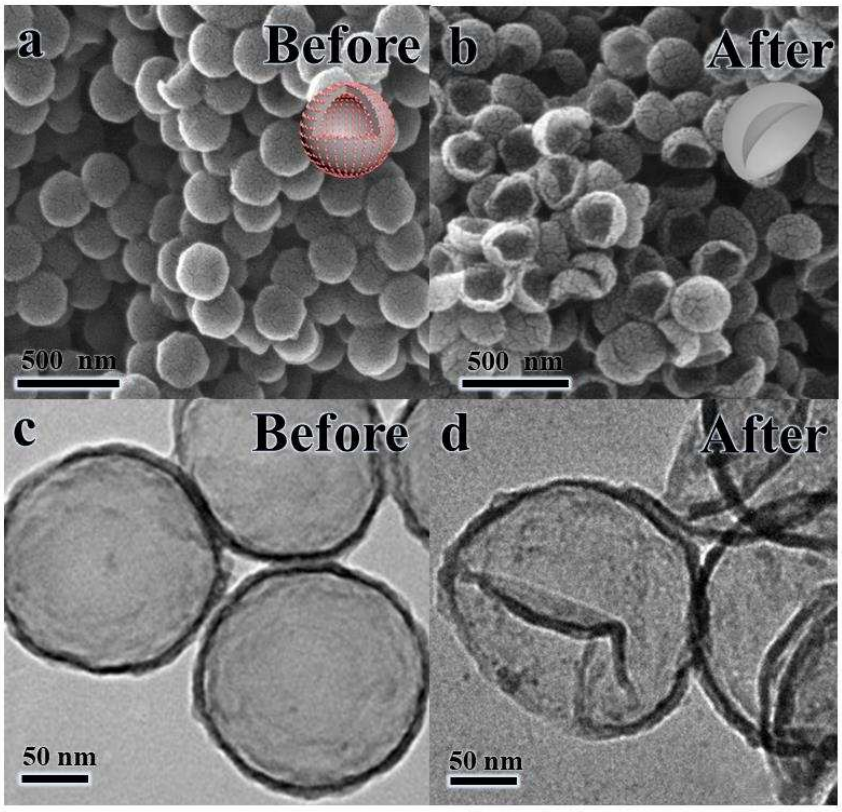

Figure 2. **SEM and TEM images of (a) and (c): HCSs before the compression showing intact morphology; (b) and (d): resultant BHCSs after the compression at 11 Mpa.**

We assume that, the different morphologies of HCSs and coresponding BHCSs prerapred with and wihtout PVP may result from the possible change in the mechinal properties induced by the introduction of PVP. Furthermore, an understanding of the mechanical property of HCSs prepared

with and without PVP is of paramount importance for exploring their practical applications. Therefore, we have investigated the mechanical performance of HCSs via the nanoindentation. Nanoindentation is an effective and convenient method for determining local mechanical properties of materials,[32-34] for example, the indentation behaviour of carbon microspheres was recently examined by Sun et. al.[33]

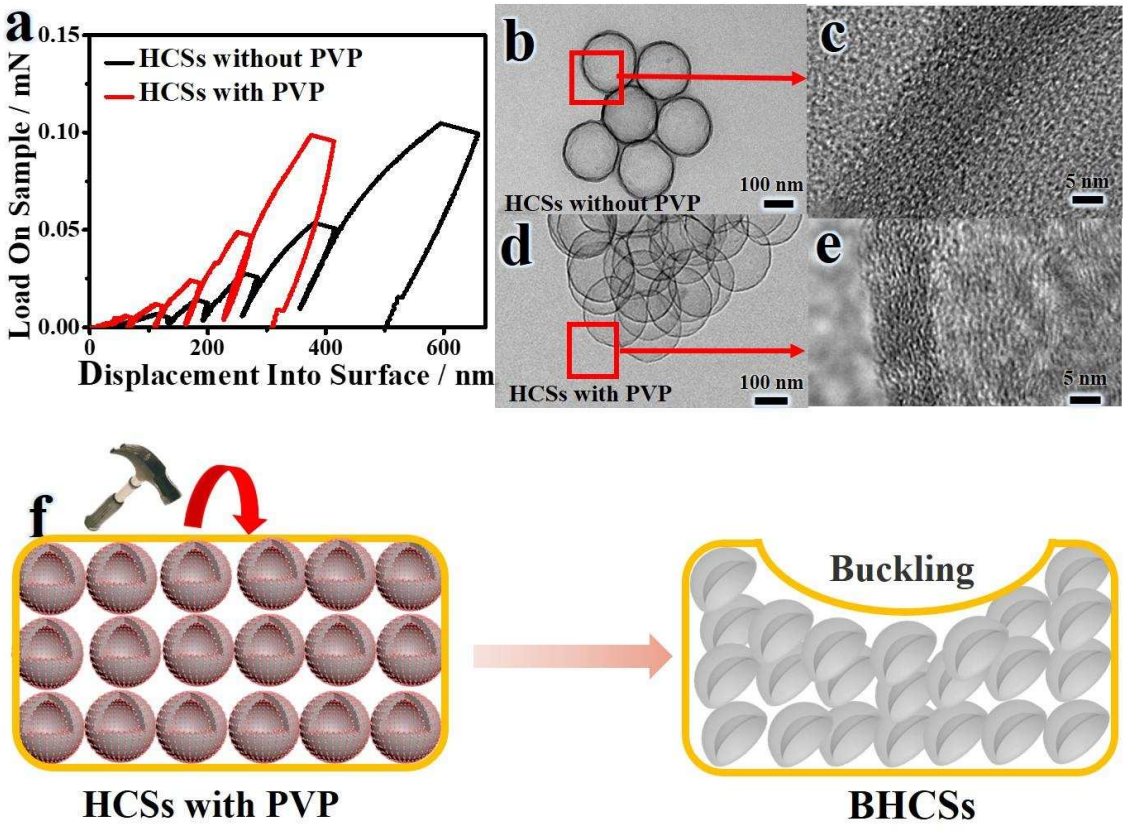

Figure 3. **(a): Loading-unloading curves for the indentation of the film made of HCSs with or without PVP; TEM (b) and HRTEM (c) image of HCSs without PVP; TEM (d) and HRTEM (e) image of HCSs with PVP; (f): Schematic depiction of the compression mode.**

In this study, the contact modulus of HCSs film was determined by nanoindentation experiment. The preparation of the films and the nanoindentation experiment are described in experimental section. The collective mechanical response of the films is probed via a spherical indenter with a radius of R_d = 80 nm, which is the same as the radius of the constituent particle. During an indentation test, the indenter was pushed onto the surface of a film made of HCSs, producing elastoplastic and plastic deformation during the loading phase. After reaching the pre-determined indentation load (0.00625, 0.0125, 0.025, 0.05, 0.1 mN), the indentation load on the indenter was maintained for 2 s, and then the indenter was retracted. **Figure 3a** shows the loading-unloading curves for the indentation of films of HCSs with and without PVP, respectively. All loading-unloading curves feature the same trend of a nonlinearly increasing force as the penetration deepens. The effective Young's modulus was 0.720 and 1.56 GPa and the hardness was 0.02 GPa and 0.03 GPa for films of HCSs prepared without PVP and with PVP respectively. Both the contact modulus and indentation hardness for the HCSs with PVP are larger than the corresponding values for the HCSs without PVP. These results show that the HCSs prepared with PVP exhibit a larger resistance to the mechanical deformation than those without PVP. Such behaviors may arise from the difference in the microstructure. Both HRTEM images and X-ray diffraction (XRD) pattern (Figure S7) suggest that HCSs with or without PVP are amorphous. However, the HCSs with PVP may have a more compacted structure and thinner shell thickness than that of the HCSs prepared without PVP, giving rise to enhanced resistance to elastic deformation (**Figure 3b and d**). The denser structure and thinner shell thickenss of HCSs with PVP were demonstrated by TEM and high resolution TEM (HRTEM) images (**Figure 3c and e**), which result from anchoring and directing effect of PVP chains for the growth of PPy precursor.

The schematic depiction of the compression mode is shown in **Figure 3f**. In order to better understand the reason of buckling process, we modeled the deformation of one hollow sphere during contact with another sphere through finite element (FE) simulation. One sphere was subjected to the indentation by a spherical indenter with same diameter in order to simulate the contact between spheres. The applied contact force was estimated based on the tablet pressure (See experimental method **Figure S12**). From the simulation results, it can be seen that at all four applied pressure (8 MPa, 11 MPa, 15 MPa and 20 MPa), the corresponding force can only result in a dimple on the surface of the sphere, but not sufficiently large to make the hollow sphere deform to form a buckled shape (**Figure 4a**) as observed in SEM images in **Figure 2** and **S6**. Notably, the Young's modulus obtained though nanoindentation is smaller than that of a single HCS (**See Methods for details**), and has been used as the lower limit of Young's modulus for FE analysis (FEA). The results have shown that, even under the condition of the lower limit of the Young's modulus, pure external load does not cause large enough deformation as observed in our experiments. Because a smaller value of Young's modulus corresponds to a larger deformation, it is clear that, the contact force and plastic deformation are not the dominant causes for the formation of buckled hollow spheres. Further simulation was conducted to explore other factors contributing to the production of BHCSs.

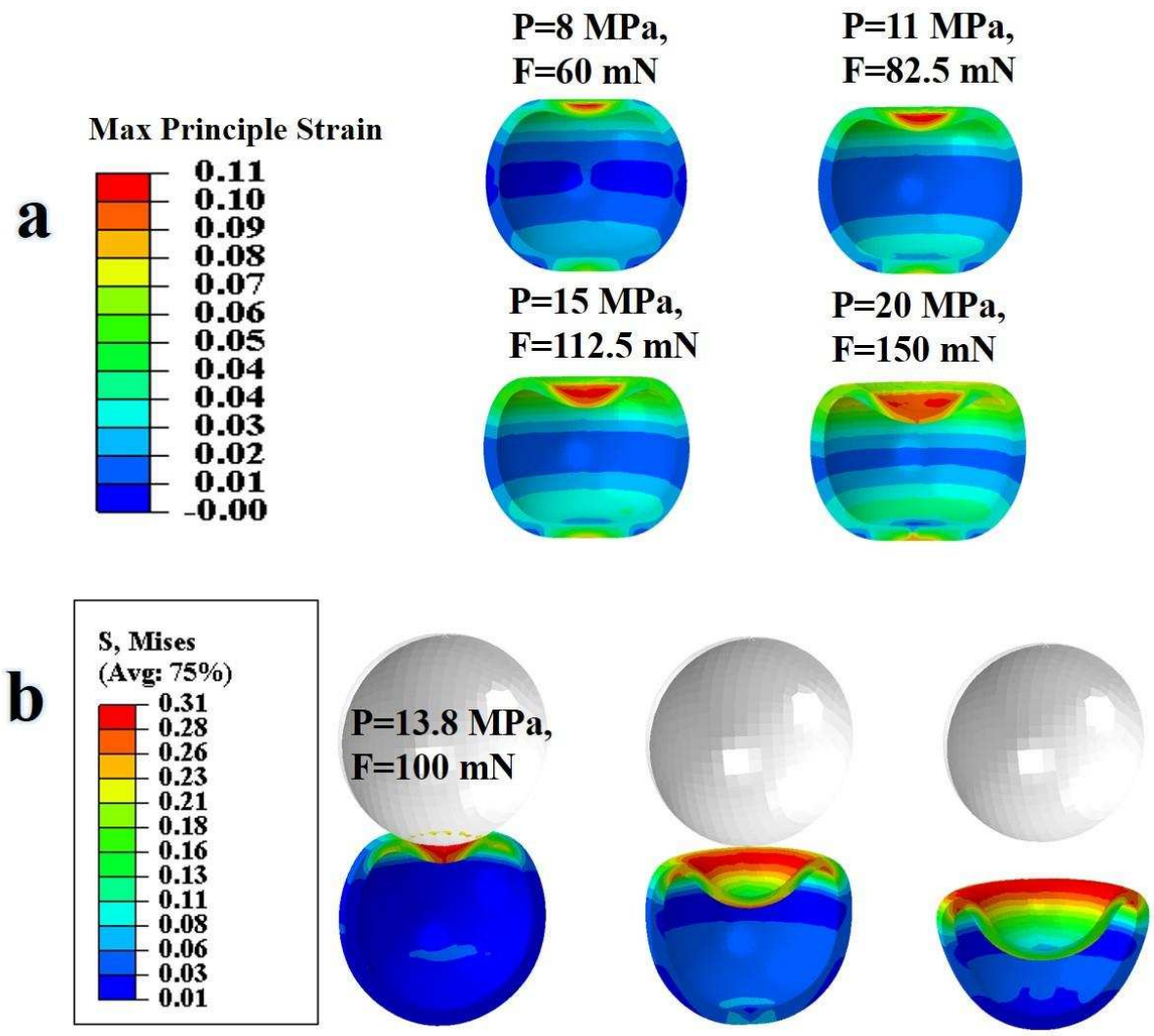

Figure 4. Cross-sectional view of FEM simulation of an individual hollow sphere subjected to the indentation by a rigid sphere with same diameter without residual stress (a) and with residual stress (b). The pressure of tablet press P on 10 mg spheres was converted to the force F on an individual sphere (13.8 MPa, 100 mN).

Interestingly, when a residual stress (9 MPa) was introduced in the process of simulation, buckled spheres are easily formed at the applied pressure (13.8 MPa, 100 mN) (Figure 4b). From Figure 4b, it can be seen that, once buckling of the shell occurs at the applied pressure, the post-buckling

of hollow sphere readily takes place without further applied pressure. According to these simulated results, we speculate that HCSs with PVP may have a residual stress, which results from the pyrolysis of both PPy and PVP. The different decomposition and contract speed contributed to the residual stress, while pyrolysis of PPy alone can not provide the residual stress. Therefore, the introduction of PVP plays a vital role in the formation of BHCSs.

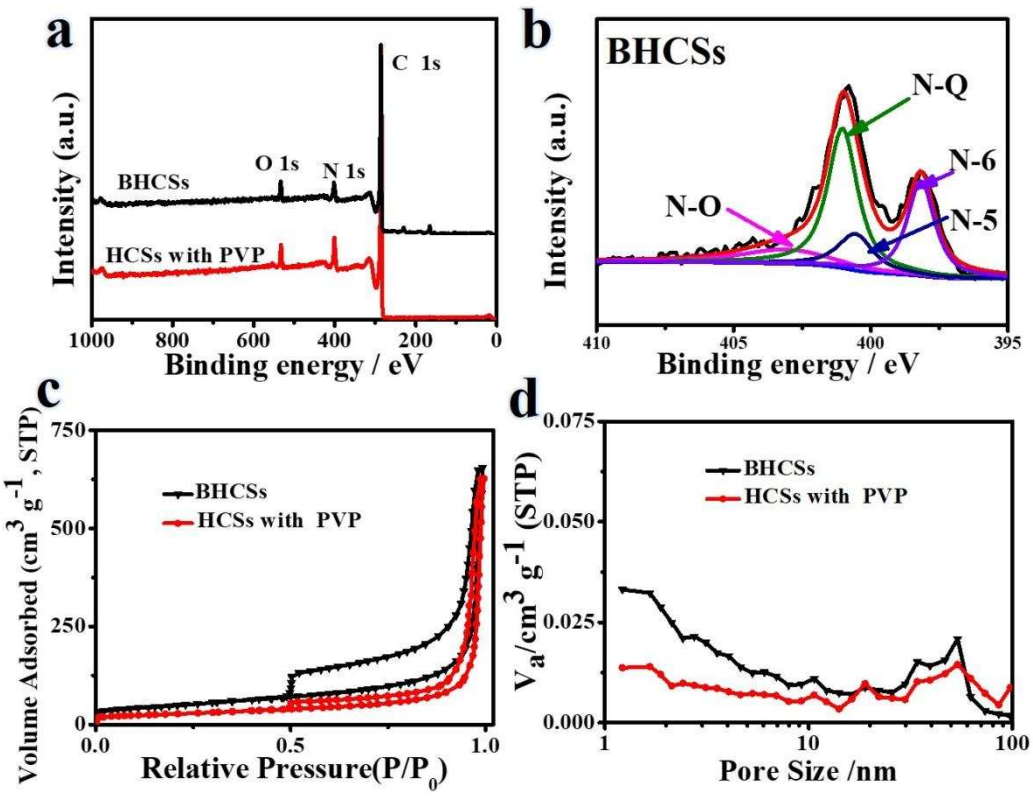

Figure 5. (a) Survey spectra of HCSs and corresponding BHCSs with PVP. (b) Representative high-resolution N1s XPS spectra of BHCSs with PVP. (c) Nitrogen adsorption-desorption isotherms of HCSs and corresponding BHCSs with PVP. (d) Pore size distributions of HCSs and corresponding BHCSs with PVP.

Both experiments and DFT calculations have revealed that nitrogen and oxygen have an active effect on improving the energy storage ability.[35] To investigate the content and distribution of nitrogen in the as-synthesized HCSs with PVP and corresponding BHCSs, XPS and EA were further utilized.[36] The results show that BHCSs show the same chemical structure as HCSs, which means that the compression method does't affect the chemical structure of sample. The percentage of the elements of C, N, H, and O in Table S1 shows that, the heteroatom content (N + O) of each sample reaches 10%. The high oxygen and nitrogen content may result from KPS, SDS, PVP and PPy. As shown in **Figure 5**, C1s, N1s, O1s peaks are all present in HCSs and BHCSs. The high resolution of O1s spectrum in Figure S7 shows the presence of oxygen-containg groups including C–O–C ether groups, C=O quinone type groups, and/or C–OH phenol groups. Figure 5b depicts the N1s spectrum (**Figure 5b**), which is fitted by four peaks, attributed to graphitic N (N-Q), pyrrolic N (N-5), pyridinic N (N-6) and oxidized N (N-O). The content of graphitic nitrogen (N-Q) and pyridinic N (N-6) is higher than other nitrogen groups for HCSs prepared with PVP, implying high degree of graphitization and the abundance of pyridinic N, which are favorable for improving both electrochemical performance and mechanical properties. It is believed that, pyridinic-N plays a role of amplifying the specific capacitance of N-doped materials because of their pseudo-capacitive contribution, and graphitic N can enhance the electrical conductivity and thus improve the capacitance performance.[37,38] Furthermore, the appropriate nitrogen and oxygen doping can reduce the resistance of electrode materials by enhancing the surface wettability with aqueous electrolyte.[39,40]

The nitrogen adsorption-desorption isotherms of HCSs and corresponding BHCSs prepared with and without PVP are shown in **Figure 5**. Each curve shows a hysteresis loop, indicating the mesoporous structure of the capsule shell. The isotherms of HCSs and corresponding BHCSs are

type-V curves as defined by International Union of Pure and Applied Chemistry (IUPAC) classification. As shown in **Figure 5c**, the nitrogen adsorption isotherms of HCSs and corresponding BHCSs exhibit a plateau at low relative pressure (P/P0<0.001) and a steep rise at high pressure (P/P0=1), which reflects microporous and macroporous structure, respectively. BHCSs process a higher SSA (170 m^2/g), almost twice as that of HCSs (96 m^2/g). This remarkable increase is asscribed to the fact that the compression has caused local fractures, generating pores on the shell of BHCSs, making the inner surface accessible. The presence of local fractures and pores on the shell is evidenced by the structural defects (some of them are indicated by red arrows) in the SEM image (**Figure S8**), as well as the increased pore volumes measure by BET (0. 886 cm^3/g for BHCSs, and 0. 867 $cm^3/$ g for HCSs, **Table S1**). Furthermore, the increased porosity of the shell can promote the transport of ions and electrons. The subtantianlly enlarged surface area, and facilitated transport of ions and electrons are expected to be beneficial for various applications.[2,41] It is noteworhty that, BHCSs prepared at a higher pressure (15MPa or 20 MPa) display lower SSAs compared with those prepared at 11MPa (Figure S9). The larger compression produces two opposing effects on the SSA of BHCSs. On one hand, it leads BHCSs to be more compactly packed with reduced gaps and more contact/overlap areas, decreasing the acessessable surface areas of BHCSs. On the other hand, it causes the fracture of particles and results in an increase of SSA. The results of SSA measurements reveal that, in our system, the former plays the predominat role in determing the SSA of obtaind BHCSs.

Electrochemistry performance of HCSs and BHCSs. Encouraged by large SSA (**Figure 5 and Table S1**) and high heteroatoms contents of HCSs and corresponding BHCSs with PVP, we tested their applications in energy storage. Cyclic voltammetry (CV) results of HCSs and BHCSs at different scanning rate in the three electrodes testing measurements are shown in **Figure S10**. All

CV curves (Figure S10a-d) display a quasi-rectangular symmetrical shape showing the behavior of electrical double-layer capacitors (EDLCs), and the CV curve area of BHCSs is larger than that of HCSs indicating the higher capacitance, which results from the increased BET of BHCSs. Meanwhile, when the scan rates are increased to 200 mV s^{-1}, the curves don't exhibit fusiform shapes due to the good ability of the sample responding to the largecurrent density due to the N and O elements.[42]

The galvanostatic charge/discharge curves (**Figure S11a-d**) corrobrate the CV results.The capacitances of HCSs and corresponding BHCSs at different charge/discharge current density are summarized in **Table. S2** and **Figure 6a**. According to the calculation, BHCSs own larger capacitance of 123 F g^{-1} than that of HCSs (101 F g^{-1}), mainly owing to the increased BET area and mesoporous structure structures of BHCSs.[43,44] Furthermore, the specific capacitance decreases when the current density is increased, which is a typcial characteristic of pseudocapacitive electrodes.[45] Figure 6b shows nyquist plots of HCSs and BHCSs. It can be seen that BHCSs displays the lower equivalent series resistance (ESR) than that of HCSs, suggesting excellent electrical conductivity coupled with improved interfacial elecrical contact between BHCSs and Ni collector. In addition, we also measured the capacitance of the samples prepared with varied pressures, finding that BHCSs prepared at 11 MPa exhibit the optimal capacitance (**Figure S10 and 11**). This is rationalized by noting that the pressure of 8 MPa does not cause obvious buckling (Figure S6), and the compression with the pressure 15 or 20 MPa has led to the reduced SSA of BHCSs compared with those prepared at 11MPa (as discussed above).

Power density (*P*) and energy density (*E*) are important parameters for evaluating the device, hence we used a two-electrode cell to calcuate E and P (details are shown in experiement part), from the curve of galvanostatic charge/discharge process with following equations:

$$C = \frac{I\Delta t}{m\Delta V} \quad (1)$$

$$E = \frac{1}{2} \times C \times (\Delta V)^2 \quad (2)$$

$$P = \frac{E}{\Delta t} \quad (3)$$

where C represents specific capacitance (F g^{-1}), I is current (A) during scanning, Δt is current drain time of discharging (s), *m* is total mass of the active material (g), and ΔV is the potential window (1 V in this work). **Figure 6c** shows ragone plots of different systems, revealing that BHCSs based device can provide an energy density as high as 41.4 Wh kg^{-1}, which is better than that of supercapacitors based on other carbon materials (All reference results are presented in **Figure 6c**). According to the comparison of the gravimetric and volumetric energy densities of different devices (**Figure 6d**), the BHCSs also exhibit a higher volumetric energy density of 46.6 Wh L^{-1}. The optimisedperformance of BHCSs can be ascribed to their higher BET surface area than HCSs, which effectively facilitates the transport of ions and eletrons in electrodes and at the electrode/electrolyte interface. Importantly, as shown in **Figure S12**, the capacitance retentions of supercapacitor with HCSs and BHCSs after 10000 cycles are 93.3% and 94.5%, respectively. These results demonstrate the prominent electrochemical durability and reproducibility of BHCSs as the electrode for supercapacitors.

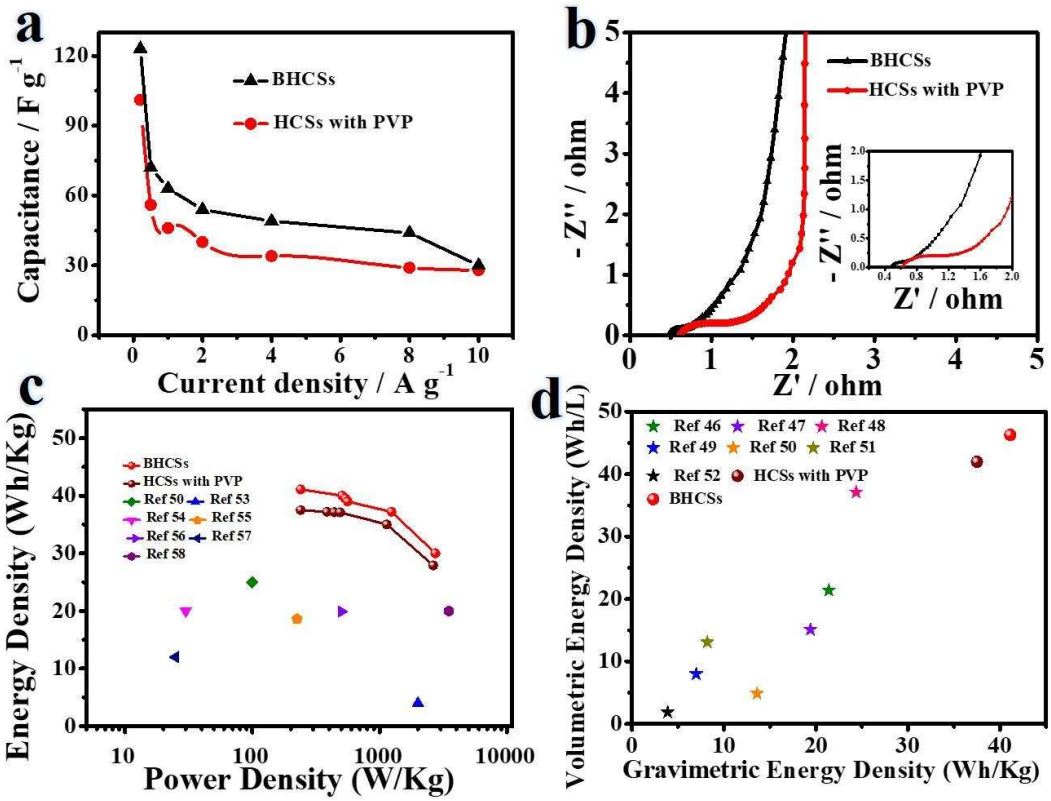

Figure 6. (a) Capacitance of HCSs and BHCSs as a function of current densinty in the range of 0.2 A g^{-1} -10 A g^{-1}. (b) Nyquist plots of all samples in the frequency range of 0.01- 100 kHz, in the eletrolyte of KOH (6M) (inset: enlarged view). (c) Ragone plot of HCSs and BHCSs and supercapacitors based on other carbon materials . (d) Comparison of the gravimetric and volumetric energy densities of different devices based on carbon electrode materials.

CONCLUSIONS

In summary, we have successfully prepared BHCSs via a simple compression method, relying on the bucking of robust HCSs. HCSs prepared with PVP demonstrated increased contact modulus and indentation hardness, which contributed to the structural durability under the compression

force. In addition, FE simulation reveals that, the residual stress, induced by the co-presence of PPy and PVP, is the key factor for the buckling process to produce BHCSs. We envisage that these BHCSs will be suitable for a broad spectrum of applications benefiting from their structural features, such as improved volumetric packing density. Our work offers valuable insights in the fabrication-property-function relationship of (buckled) HCSs, in terms of adjusting the compactness of the carbon precursor, enhancing the mechanical modulus, and improving the capacitance as supercapacitors, and hence opens up an avenue for engineering well-defined hollow nanostructures with structural integrity and durability.

METHODS

Chemicals.The styrene (St) monomer (Sinopharm Chemical Reagent Co, A.R.) was rinsed with an aqueous solution of sodium hydroxide, and then distilled under reduced pressure. Pyrrole (Py) (Aldrich, 99%) was distilled to remove impurities and stored in a cryogenic environment protected with nitrogen. Iron (III) chloride hexahydrate ($FeCl_3 \cdot 6H_2O$, 98%), hydrochloric acid, ethanol, sodium dodecyl sulfate (SDS), potassium persulfate (KPS), polyvinylidene fluoride (PVDF), polyvinylpyrrolidone (PVP, MW:1300000) polytetrafluoroethylene (PTFE), and N-methyl 2-pyrrolidone (NMP), carbon black were all purchased from Sinopharm Chemical Reagent Co and used as received.

Preparation of PS NPs. The synthesis of PS NPs follows our previous work.[25] The resultant PS latexes have a particle size of (150± 8.8 nm).

Fabrication of Core-shell NPs. A typical procedure of synthesizing PS@ PPy/PVP core-shell NPs is described as follows: 0.5 g PS NPs and 0.1 g PVP were dispersed in 30 ml deionized water

and deoxygenated for 90 min, followed by the introduction of Py monomer 0.4. Then $FeCl_3 \cdot 6H_2O$ (2.7 g/5 ml) aqueous solution was drop-wise added to the reaction mixture for about 2 min with stirring. Following the 24-hour polymerization at room temperature, the products were centrifuged, rinsed by several cycles with water, diluted hydrochloric acid and alcohol. At last, the samples were dried at 65 ºC under vacuum. PS@PPy core-shell NPs without PVP were prepared in the same procedure for control purpose.

Fabrication of Carbonized samples. The obtained core-shell NPs were carbonized under nitrogen atmosphere to fabricate HCSs. The procedure follows our previous work.[31] HCSs without PVP were prepared in the same procedure for control purpose.

Fabrication of BHCSs. BHCSs were obtained by compressing HCSs with and without PVP at 6~20 MPs with a mechanical press.

Characterization. Scanning electron microscopy (SEM) imaging was performed on Quanta 400 FEG. Transmission electron microscope (TEM) imaging was conducted on a FEI Tecani G2 F20 S-TWIN. X-ray diffraction (XRD) analysis was performed on X'Pert-Pro MPD diffractometer with a Cu Kα radiation source at room temperature (the angle measurement accuracy is 0.02°). X-ray photoelectron spectroscopy (XPS) measurements were carried out by using an ESCALAB 250 instrument (Thermo Electron) with Al Kα radiation. Element analysis (EA) was performed using Vario EL cube. The nitrogen adsorption–desorption isotherms were collected at 77 K using NOVA 2000 (Micromeritics ASAP 2020). Before the investigation of the textural properties with nitrogen sorption technique, the samples were degassed for 5 h at 70 ºC. The specific surface area was calculated using the BET (Brunauer-Emmet and Teller) model, while the pore size and pore volume were calculated using the Barrett–Joyner–Halenda (BJH) formula according to the

desorption branch of the isotherm. Mechanical properties were evaluated by a nanoindenter (Nano Indenter G200) using a Berkowich diamond tip, which was a three-sided pyramid with a radius of 80 nm. The film of HCSs was prepared by mixing PVDF, HCSs, and NMP at the weight ratio of (1:1:10) and dried at 80 ^{o}C. Loading-unloading curves were recorded, from which the indentation depth and indentation load were used to calculate the contact modulus and indentation hardness of the HCSs films. The indentation load was 0.00625, 0.0125, 0.025, 0.05, 0.1 mN. Two indents were performed for each experimental condition. All measurements were performed in duplicate. The two points are 30 μm apart.

Finite element (FE) modeling. Finite element simulation was conducted using commercial software ABAQUS/Explicit. For simplicity, HCSs were modeled as linear elastic material. The Young's modulus of HCSs was set to be 1.56 Gpa as estimated from nanoindentation test and Possion's ratio was set to be 0.4.[59] It is important to note that, to analyze nanoindentation data, the array of nanoparticles was considered as a continuous film to fit with existing model and an equivalent modulus was calculated. The Young's Modulus (1. 56 GPa) obtained via this method represents the collective stiffness of multi-layer array of hollow spheres, and was previously reported to be smaller than the Young's Modulus of monolayer of close-packed hollow spheres measured using nanoindentation,[60] which was demonstrated to represent the intrinsic Young's modulus of the constituent individual hollow nanosphere.[59] Therefore, the Young's modulus obtained though nanoindentation is considered to be smaller than that of a single HCS and used as the lower limit of Young's modulus in FEA. The outer radius of hollow sphere was 85 nm and the thickness of shell was 11 nm. The HCSs were modelled using C3D6 elements. The whole set up of simulation was shown in Figure S13. In order to model the deformation of an individual HCS induced by contact and interaction with other hollow spheres, the tested hollow sphere was

supported by a rigid plane and subjected to the indentation with a rigid ball of the same diameter. A concentrated force was calculated from pressure and applied to the spherical indenter. The force applied on each individual sphere during compression can be estimated by $F_{all} = P * A$, where P is the pressure read from tablet press and A is the projected area of a sphere. Suppose the spheres are packed as HCP or FCC, each sphere on one layer is in contact with three spheres on the next layer and transmitted the force. Therefore, each contact between two spheres shares approximately 1/3 overall force bear by one sphere, e.g., $F = \frac{F_{all}}{3} = \frac{PA}{3} \approx PR^2$, where R is the outer radius of HCSs.

Three-Electrode Testing Measurements. A three-electrode configuration was applied to investigate the electrochemical performance of obtained samples, with the following procedure: first, HCSs or BHCSs were mixed with carbon black and PTFE binder with a weight ratio of 8:1:1. Secondly, the mixtures were painted and pressed on the collector. The detailed procedures are presented in our published work.[31] The tests were performed on an electrochemical workstation (CHI660E) in 6 M KOH aqueous electrolyte solution at room temperature.

Two-Electrode Tests. The symmetrical two-electrode coin supercapacitor was manufactured in a dry environment at room temperature. The two electrodes were separated by a filter paper soaked with 1M sodium sulfate. The working electrode was fabricated by mixing HCSs or BHCSs, PVDF and carbon black at the ratio of 8:1:1 in the solvent of NMP to obtain a homogeneous slurry, then the symmetrical two-electrode testing coin supercapacitor was prepared. The typical mass loading on one electrode was around 2.5 mg cm^{-2}, and the thickness of electrode was controlled to be about 30 μm. The electrochemical characterizations were performed on a CHI660E electrochemical workstation at 25 ºC.

ASSOCIATED CONTENT

Supporting Information

The Supporting Information is available free of charge on the ACS Publications website.

SEM and TEM images HCSs prepared with different contents of PPy, characterization of PS NPs, TEM images of HCSs without or with PVP, TGA curve of PVP, Figure S5. SEM and TEM images of HCSs without PVP before and after the compression at 11 MPa, SEM images of BHCSs prepared via the compression at different pressures, XRD patterns and XPS results of BHCSs and HCSs, parameters on surface area, pore structures and elemental composition of HCSs and BHCSs, CV curves and Galvanostatic charge/discharge curves of HCSs and BHCSs prepared with different pressures, specific capacitance of the HCS materials, Charge/discharge cycle of HCSs and BHCSs, and Set up of the Finite element simulation.

AUTHOR INFORMATION

Corresponding Author

* E-mail: S.Ye@leeds.ac.uk (S. Ye)

* E-mail: yangxiaoming@suda.edu.cn (X. Yang).

Author Contributions

The manuscript was written through contributions of all authors. All authors have given approval to the final version of the manuscript. ‡These authors contributed equally.

Notes

The authors declare no competing financial interest.

ACKNOWLEDGEMENTS

The authors would like to thank the following for financial support: National Natural Science Foundation of China (No. 21104050), the China Postdoctoral Science Foundation (2013M541715, 2014T70541), a project funded by the Priority Academic Program Development of Jiangsu Higher Education Institutions (PAPD), the fund (2017002) from the Key Laboratory of Advanced Textile Materials and Manufacturing Technology (Zhejiang Sci-Tech University), the Ministry of Education, the Fundamental Research Funds for the Welcome Trust ISSF Junior Investigator Development Fellowship. The authors thank Lucien Roach for proof-reading.

REFERENCES

(1) Lin, T.; Chen, I. W.; Liu, F.; Yang, C.; Bi, H.; Xu, F.; Huang, F. Nitrogen-Doped Mesoporous Carbon of Extraordinary Capacitance for Electrochemical Energy Storage. *Science* **2015**, *350*, 1508-1513.

(2) Liang, J.; Yu, X. Y.; Zhou, H.; Wu, H. B.; Ding, S.; Lou, X. W. Bowl‐Like SnO_2@ Carbon Hollow Particles as an Advanced Anode Material for Lithium-Ion Batteries. *Angew Chem. Int. Ed. Engl*. **2014**, *53*, 12803-12807.

(3) Liang, J.; Hu, H.; Park, H.; Xiao, C.; Ding, S.; Paik, U.; Lou, X. Construction of Hybrid Bowl-Like Structures by Anchoring Nio Nanosheets on Flat Carbon Hollow Particles with Enhanced Lithium Storage Properties. *Energy & Environ. Sci.* **2015**, *6*, 1707-1711.

(4) Hosein, I. D.; Liddell, C. M. Convectively Assembled Nonspherical Mushroom Cap-Based Colloidal Crystals. *Langmuir* **2007**, *23*, 8810-8814.

(5) Titirici, M. M.; Antonietti, M. Chemistry and Materials Options of Sustainable Carbon Materials Made by Hydrothermal Carbonization. *Chem. Soc. Rev.* **2010**, *39*, 103-116.

(6) Lee, J.; Kim, J.; Hyeon, T. Recent Progress in the Synthesis of Porous Carbon Materials. *Adv. Mater*. **2006**, *18*, 2073-2094.

(7) Li. S.; Pasc. A.; Fierro. V.; Celzard, A. Hollow Carbon Spheres: Synthesis and Applications-A Review. *J. Mater. Chem. A*. **2010**, *4*, 12686-12713.

(8) Lin, T.; Chen, I. W.; Liu, F.; Yang, C.; Bi, H.; Xu, F.; Huang, F. Nitrogen-Doped Mesoporous Carbon of Extraordinary Capacitance for Electrochemical Energy Storage. *Science* **2015**, *350*, 1508-1513.

(9) Liang, J.; Yu, X. Y.; Zhou, H.; Wu, H. B.; Ding, S.; Lou, X. W. Bowl- Like SnO_2@Carbon Hollow Particles as an Advanced Anode Material for Lithium- ion Batteries. *Angew Chem. Int. Ed. Engl*. **2014**, *53*, 12803-12807.

(10) An, Q. F.; Qian, J. W.; Zhao, Q.; Gao, C. J. Polyacrylonitrile-Block-Poly (Methyl Acrylate) membranes 2: Swelling Behavior and Pervaporation Performance for Separating Benzene/Cyclohexane. *J. Membrane Sci.* **2008**, *313*, 60-67.

(11) Liang, J.; Yu, X. Y.; Zhou H.; Wu, H. B.; Ding S.; Lou, X. W. Construction of Hybrid Bowl-Like Structures by Anchoring NiO Nanosheets on Flat Carbon Hollow Particles with Enhanced Lithium Storage Properties. *Energy & Environ. Sci.* **2015**, *8*, 1707-1711.

(12) Huang, Y. J., Zhou, J., Xu L., Li, Z., Zhang, Y., Wang, J., Song, Y., Jiang, L., Controllable Synthesis of Latex Particles with Multicavity Structures. *Macromolecules* **2011**, *44*. 2404-2409.

(13) Hu, X.; Dou, Y.; Li, J.; Liu, Z. Buckled Structures: Fabrication and Applications in Wearable Electronics. *Small* **2019**, 1804805

(14）Liu, Z. F.; Fang, S.; Moura, F. A.; Ding, J. N.; Jiang, N.; Di, J.; Yuan, N. Y. Hierarchically Buckled Sheath-core Fibers for Superelastic Electronics, Sensors, and Muscles. *Science* **2015**, *349*, 400-404.

(15) Run, W.; Liu, Z. S.; Wan, G.Y.; Jia, T. J.; Zhang, C.; Wang, X.M.; Zhang, M.; Qian, D.; Jiang, N.; Yin,S. J.; Zhang,R.;Feng, D.Q.; Wang, W. C.; Zhang, H.; Chen, H.; Wang,Y.S.; Raquel, O.; Inoue, K.; Lu, H. B.; Fang, S. L.; Baughman, R. H.; Liu, Z. F. Controllable Preparation of Ordered and Hierarchically Buckled Structures for Inflatable Tumor Ablation, Volumetric Strain Sensor, and Communication via Inflatable Antenna. *ACS Appl. Mater. Interfaces* **2019**, *11*, 10862-10873

(16) Ohta, T.; Nagao, D.; Ishii, H.; Konno, M. Preparation of Oil-Containing, Polymeric Particles Having a Single Depression with Various Shapes. *Soft Matter.* **2012**, *8*, 4652-4658.

(17) Xu, X.; Asher. S. A. Synthesis and Utilization of Monodisperse Hollow Polymeric Particles in Photonic Crystals. *J. Am. Chem. Soc.* **2004**, *126*, 7940-7945.

(18) Donath, E.; Sukhorukov G. B.; Caruso, F.; Davis, S. A.; Möhwald, H. Novel Hollow Polymer Shells by Colloid-Templated Assembly of Polyelectrolytes. *Angew Chem. Int. Ed.* **1998**, *37*, 2201-2205.

(19) Yang, W.; Mao, S.; Yang, J.; Shang, T.; H. J. Song.; W. Mabon.; Vance J.; Yue. Z.; Dillon. S.; Xu. B.; Xu. H. Large-Deformation and High-Strength Amorphous Porous Carbon Nanospheres. *Sci. Rep*. **2016**, *6*. 24187.

(20) Wu, Y.; Alici, G.; Madden, J. D.; Spinks, G. M. Wallace, G. G. Soft Mechanical Sensors through Reverse Actuation in Polypyrrole. *Adv. Funct. Mater.* **2007**, *17*, 3216-3222.

(21) Deng, T. S.; Marlow, F. Synthesis of Monodisperse Polystyrene@Vinyl-SiO_2 Core–Shell Particles and Hollow SiO_2 Spheres. *Chem. Mater.* **2012**, *24*, 536-542.

(22) Roberts, A. D.; Li, X.; Zhang, H. Porous Carbon Spheres and Monoliths: Morphology Control, Pore Size Tuning and Their Applications as Li-Ion Battery Anode Materials. *Chem. Soc. Rev.* **2014**, *43*, 4341-4356.

(23) Nair, K. M.; Thomas, S.; Groeninckx, G. Thermal and Dynamic Mechanical Analysis of Polystyrene Composites Reinforced with Short Sisal Fibres. *Compos. Science. Technol*. **2001**, *61*, 2519-2529.

(24) Xia, Y.; Wei, M.; Lu, Y. One-Step Fabrication of Conductive Poly (3, 4-Ethylenedioxythiophene) Hollow Spheres in the Presence of Poly (Vinylpyrrolidone). *Synth. Met.* **2009**, *159*, 372-376.

(25) Yang, X.; Ge, D.; Wu, G.; Liao Z.; Yang, S. Production of Structural Colors with High Contrast and Wide Viewing Angles from Assemblies of Polypyrrole Black Coated Polystyrene Nanoparticles. *ACS Appl. Mater. Interface* **2016**, *8*, 16289-16295.

(26) Ge, D.; Yang X.; Chen, Z.; Yang, L.; Wu, G.; Xia, Y.; Yang, S. Colloidal Inks from Bumpy Colloidal Nanoparticles for the Assembly of Ultrasmooth and Uniform Structural Colors. *Nanoscale* **2017**, *9*, 17357-17363.

(27) Li, W.; Zheng, G.; Yang, Y.; She, Z. W.; Liu, N.; Cui, Y. High-Performance Hollow Sulfur Nanostructured Battery Cathode through A Scalable, Room Temperature, One-Step, Bottom-Up Approach. *P. Natl. A. Sci. India. A.* **2013**, *110*, 7148-7153.

(28) Molyneux, P. Water-Soluble Synthetic Polymers: Volume II: Properties and behavior, 1st ed; CRC Press. Inc: Florida, **1983**, 146-147.

(29) Betti, N. A. Thermogravimetric Analysis on PVA/PVP Blend under Air Atmosphere. *Eng. & Tech. Journal.* **2016**, 3*4*, 2433-2442.

(30) Ge, Y.; Chen, Z.; Ye, S. J.; Zhu, Z. F.; Tu, Y. F.; Yang, X. M. A Spheres-in-Tube Carbonaceous Nanostructure for High-Capacity and High-Rate Lithium–Sulfur Batteries. *J. Mater. Chem. A.* **2018**, *6*,14885-14893.

(31) Chen, Z., Ye, S. J.; Evans, S. D.; Ge, Y. H.; Zhu, Z. F.; Tu, Y. F.; Yang, X. M. Confined Assembly of Hollow Carbon Spheres in Carbonaceous Nanotube: A Spheres-in-Tube Carbon Nanostructure with Hierarchical Porosity for High-Performance Supercapacitor. *Small* **2018**, *14*, 1704015.

(32) Sun, Y.; Chen, R.; Zhao, G.; Yang, F. J. Nano Indentation of Carbon Microspheres: Paper Presented at the Symposium. *J. Mater. Res*. **2016**, *107*, 687-691.

(33) Liu, Y.; Wang, D.; Shi, J.; Peng, Q.; Li, Y. Magnetic Tuning of Upconversion Luminescence in Lanthanide-Doped Bifunctional Nanocrystals. *Angew Chem. Int. Ed.* **2013**, *125*, 4462-4465.

(34) Zhang, H. S.; Komvopoulos, K. Behavior of Cu-Al-Ni Shape-Memory Alloy Induced by Partial Indentation Unloading. *Nanotech. Let.* **2010**, *2*, 332-336.

(35) Watanabe, M.; Thomas, M. L.; Zhang S.; Ueno K.; Yasuda, T.; Dokko, K. Application of Ionic Liquids to Energy Storage and Conversion Materials and Devices. *Chem. Rev*. **2017**, *117*, 7190-7239.

(36) Tan, H.; Tang, J.; Henzie, J.; Li, Y.; Xu, X.; Chen, T.; Wang, Z.; Wang, J.; Ide, Y.; Bangdo, Y.; Yamauchi, Y. Assembly of Hollow Carbon Nanospheres on Graphene Nanosheets and Creation of Iron-Nitrogen-Doped Porous Carbon for Oxygen Reduction. *ACS. Nano* **2018**, *12*, 5674-5683.

(37) Tian, H.; Lin, Z.; Xu, F.; Zheng, J.; Zhuang, X.; Mai, Y.; Feng, X. Quantitative Control of Pore Size of Mesoporous Carbon Nanospheres through the Self-Assembly of Diblock Copolymer Micelles in Solution. *Small* **2016**, *12*, 3155-3163.

(38) Zhong, H.; Zhang, H.; Liu, S. C. Deng, M. Wang, Nitrogen-Enriched Carbon From Melamine Resins with Superior Oxygen Reduction Reaction Activity. *Chem. Sus. Chem.* **2013**, *6*, 807-812.

(39) Li, W.; Chen, D.; Li, Z.; Shi.; Wan, Y.; Wang, G.; Jiang, Z.; Zhao, D. Nitrogen-Containing Carbon Spheres With Very Large Uniform Mesopores: The Superior Electrode Materials for EDLC in Organic Electrolyte. *Carbon* **2007**,*45*, 1757-1763.

(40) Wickramaratne, N. P.; Xu, J.; Wang, M.; Zhu, L.; Dai L.; Maroniec, M.; Nitrogen Enriched Porous Carbon Spheres: Attractive Materials for Supercapacitor Electrodes and CO_2 Adsorption. *Chem. Mater*. **2014**, *45*, 2820-2828.

(41) Zhang, Y.; Zhang, W.; Shen, S.; Yan, X.; Wu, A.; Yin, J.; Zhang, J. Hollow Porous Bowl-Shaped Lithium-Rich Cathode Material for Lithium-Ion Batteries with Exceptional Rate Capability and Stability. *J. Power Sources*, **2018**. *380*, 164-173.

(42) Lu, A. H.; Li, W. C.; Hao, G. P.; Spliethoff, B.; Bongard, H. J. ; Schaack, B. B.; Schüth, F. Easy Synthesis of Hollow Polymer, Carbon, Graphitized Microspheres. *Angew Chem. Int. Ed.* **2010**, *49*, 1615-1618.

(43) Zhang, C.; Lv, W.; Tao, Y.; Yang, Q. H. Towards Superior Volumetric Performance: Design and Preparation of Novel Carbon Materials for Energy Storage. *Energy Environ. Sci.* **2015**, *8*, 1390-1403.123

(44) Silva, R.; Voiry, D.; Chhowalla, M.; Asefa, T. Efficient Metal-Free Electrocatalysts for Oxygen Reduction: Polyaniline-Derived N-and O-Doped Mesoporous Carbons. *J. Am. Chem. Soc.* **2013**,*135*, 7823-7826.

(45) Tao, Y.; Xie, X.; Lv, W.; Tang, D. M.; Kong, D.; Huang, Z.; Nishihara, H.; Ishii, T.; Li, B.; Golberg, D.; Kyotani, T.; Yang, Q.; Kang, F. Towards Ultrahigh Volumetric Capacitance: Graphene Derived Highly Dense but Porous Carbons for Supercapacitors. *Sci. Rep*. **2013**, *3*, 2975.

(46) Li, N.; Ji, L.; Li, Y.; Yang, X.; Lu, Y.; Tu, Y. N-and O-Doped Carbonaceous Nanotubes from Polypyrrole for Potential Application in High-Performance Capacitance. *J. Power Sources* **2014**, *24*, 660-666.

(47) Tao, Y.; Lv, W.; Yang, Q. H. Graphene-Based Highly Dense but Porous Carbons with Ultrahigh Volumetric Capacitance for Supercapacitors. *J. Electrochem. Soc.* **2014**, *2*, 310-310.

(48) Hatzell, K. B.; Boota, M.; Dyatkin, B.; Beidaghi, M.; Long, D.; Qiao, W.; Kumbur, E.; Gogotsi, Y. Highly Porous Carbon Spheres for Electrochemical Capacitors and Capacitive Flowable Suspension Electrodes. *Carbon* **2014**, *77,* 155-164.

(49) Chen, L. F.; Zhang, X. D.; Liang, H. W.; Kong, M.; Guan, Q. F.; Chen, P.; Wu, Z. and Yu, S. H. Synthesis of Nitrogen-Doped Porous Carbon Nanofibers as An Efficient Electrode Material for Supercapacitors. *ACS Nano* **2012**, *6*, 7092-7102.

(50) Wang, Q.; Yan, J.; Wang, Y.; Wei, T.; Zhang, M.; Jing, X.; Fan, Z. T. Three-Dimensional Flower-Like and Hierarchical Porous Carbon Materials as High-Rate Performance Electrodes for Supercapacitors. *Carbon* **2014**, *67*, 119-127.

(51) Xiao, N.; Tan, H.; Zhu, J.; Tan, L.; Rui, X.; Dong, X.; Yan, Q. High-Performance Supercapacitor Electrodes Based on Graphene Achieved by Thermal Treatment with The Aid of Nitric Acid. *ACS Appl. Mater. Interface* **2013**, *5*, 9656-9662.

(52) Raymundo, P. E.; Cadek, M. Tuning Carbon Materials for Supercapacitors by Direct Pyrolysis of Seaweeds. *Adv. Funct. Mater.* **2009**, *19*, 1032-1039.

(53) Wang, K.; Huang, L.; Razzaque, S.; Jin, S.; Tan, B. Fabrication of Hollow Microporous Carbon Spheres from Hyper-Crosslinked Microporous Polymers. *Small* **2016**, *12*, 3134-3142.

(54) Lei, Z.; Zhang, J.; Zhao, X. S. Ultrathin MnO_2 Nanofibers Grown on Graphitic Carbon Spheres as High-Performance Asymmetric Supercapacitor Lectrodes. *J. Mater. Chem.* **2012**, *21*, 153-160.

(55) Li, Y.; Yu, N.; Yan, P.; Li, Y.; Zhou, X.; Chen, S.; Wang, G.; Wei, T; Fan, Z. Fabrication of Manganese Dioxide Nanoplates Anchoring on Biomass-Derived Cross-Linked Carbon Nanosheets for High-Performance Asymmetric Supercapacitors. *J. Power Sources* **2015**, *300*, 309-317.

(56) Wang, G.; Xu, H.; Lu, L.; Zhao, H. One-Step Synthesis of Mesoporous MnO_2/Carbon Sphere Composites for Asymmetric Electrochemical Capacitors. *J. Mater. Chem. A.* **2015**, *3*, 1127-1132.

(57) Arif, A. F.; Kobayashi, Y.; Balgis, R.; Ogi, T.; Iwasaki, H.; Okuyama, K. Rapid Microwave-Assisted Synthesis of Nitrogen-Functionalized Hollow Carbon Spheres with High Monodispersity. *Carbon* **2016**, *107,* 11-19.

(58) Liu, B.; Yang, M.; Chen, H.; Liu, Y.; Yang, D.; Li, H. Graphene-Like Porous Carbon Nanosheets Derived From Salvia Splendens for High-Rate Performance. *J. Power Sources* **2018**, *397,* 1-10.

(59) Yin. J.; Retsch. M.; Lee. J. H.; Thomas. E. L.; Boyce, M. C. Mechanics of Nanoindentation on a Monolayer of Colloidal Hollow Nanoparticles. *Langmuir* **2011**, *27*, 10492-10500.

(60) Yin, J.; Retsch, M.; Thomas, E. L.; Boyce, M. C. Collective Mechanical Behavior of Multilayer Colloidal Arrays of Hollow Nanoparticles. *Langmuir* **2012**, *28*, 5580-5588.

TOC:

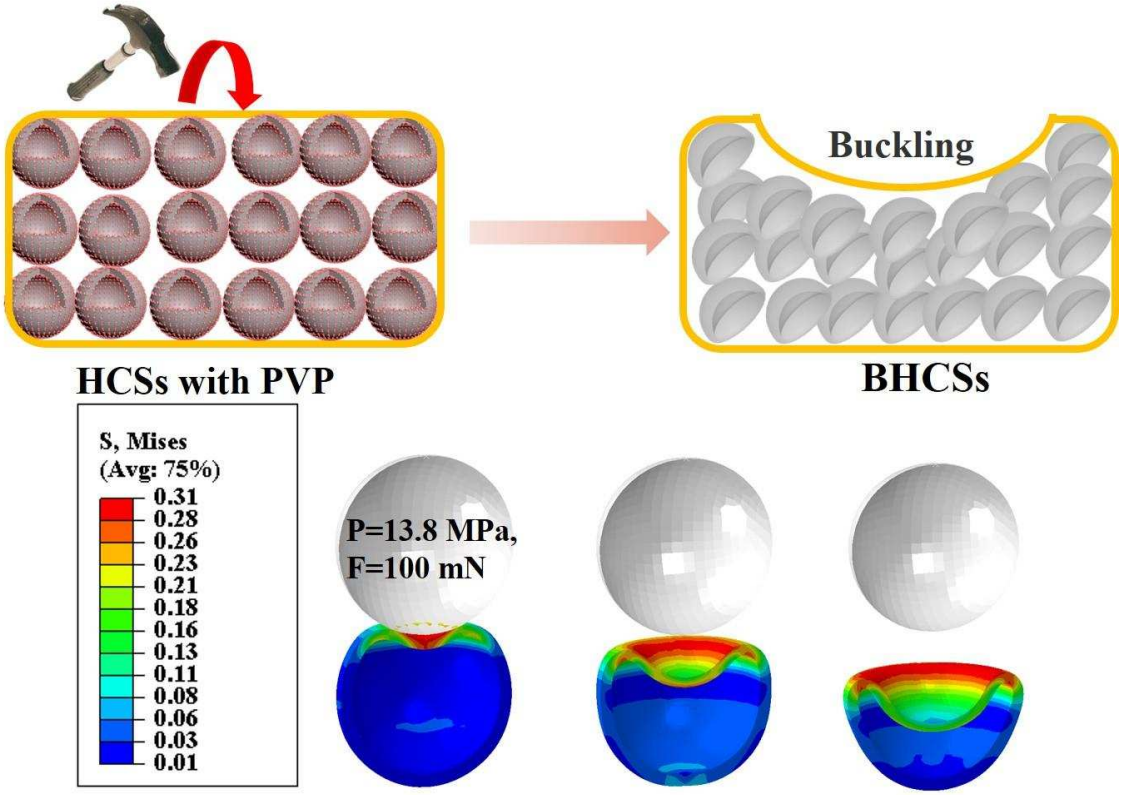
Buckling
HCSs with PVP
BHCSs
S, Mises
(Avg: 75%)
0.31
0.28
0.26
0.23
0.21
0.18
0.16
0.13
0.11
0.08
0.06
0.03
0.01
P=13.8 MPa,
F=100 mN